

UNSTEADY PARTICLE DEPOSITION IN A HUMAN NASAL CAVITY

Camby M.K. SE¹, Kiao INTHAVONG¹ and Jiyuan TU¹

¹ School of Aerospace, Mechanical and Manufacturing Engineering, RMIT University, PO Box 71, Bundoora Vic 3083, AUSTRALIA

ABSTRACT

The deposition efficiency of unsteady inhalation is investigated in present study by using computational fluid dynamics techniques. Comparison with steady inhalation is also discussed. The inspiratory cycle of a realistic unsteady inhalation profile was applied at the outlet of nasopharynx, which has the maximum flow rate of 40.3L/min. Aerodynamic particle sizes of 5 μ m and 20 μ m were studied in order to reflect a low and high Stokes numbered particle, respectively. Three profiles of particle deposition efficiency in the nasal cavity versus time are presented. In general, the total deposition of 5 μ m was found much less than 20 μ m particle. Lower deposition was achieved for 5 μ m as inhalation accelerates. The first 0.2 second of the inspiratory cycle was found to be a crucial period as majority of particles deposited during the period. These particle sizes gave the highest deposition efficiency in the middle region of the nasal cavity. However, the distribution changed for large particle under steady inhalation. Comparing with its equivalent steady inhalation flow rate, the unsteady inhalation had lower deposition efficiency for both particle sizes.

NOMENCLATURE

\vec{U}	Velocity components of fluid
k	Turbulent kinetic energy
ω	Specific dissipation rate
ρ	Density of fluid
μ	Dynamic viscosity
μ_t	Turbulent viscosity
δ_{ij}	Kronecker delta
\vec{F}	External body forces
F_D	Drag force per unit particle mass
Re_p	Particle Reynolds number
C_D	Drag coefficient

INTRODUCTION

Suspended airborne particulates are characterised by their small size and thus have a high residence time in the air. Inhalation of these particulates becomes unavoidable. Respiratory diseases such as influenza, and tuberculosis (TB), may be resulted due to excessive exposure of harmful respiratory bacteria. Deposition of harmful particulates in respiratory system can also lead to severe health complications such as lung cancer, and Mesothelioma (asbestosis). Experimental and numerical studies (Anthony and Flynn 2006; Se *et al.* 2009) have shown that facial features, such as the nose, lips, cheeks etc., are able to reduce the inhalability of airborne particles. For those inhaled particles, the nasal cavity must become another natural defence where a portion of particles will deposit before being removed by mucociliary action. Deposition of

particles in the bronchus or the alveoli which are deep in the lungs should be avoided as the particles will be accumulated and affect the functionality of the respiratory system. In light of this, many experimental and numerical studies (Balashazy and Hofmann 1993; Cheng *et al.* 1996; Moskal and Gradon 2002; Zhang *et al.* 2009) of particle deposition in the nasal cavity have been performed to study the deposition and the probability of deep particle deposition in the lung.

Particle deposition efficiency is affected by the particle size and the airflow velocity. The latter factor is referred to as the inhalation flow rate with respect to the topology of the nasal cavity geometry. Both factors have been studied experimentally and numerically (Inthavong *et al.* 2006; Shi, Kleinstreuer *et al.* 2007; Zwartz and Guilmette 2001) resulting in two general findings: 1) deposition efficiency increases with the particle size; 2) deposition efficiency decreases with increases in the inhalation flow rate. In most of these studies, a constant inhalation flow rate with a constant inlet velocity at nostril surfaces was usually adopted (Shanley *et al.* 2008; Shi, Kleinstreuer *et al.* 2007; Subramaniam *et al.* 1998). A recent in-vivo experimental work conducted by Hauermann *et al.* (2001) had highlighted that this traditional approach neglects the acceleration during inhalation and thus leads to over-predict particle deposition in comparing to a cyclic breathing pattern (i.e. unsteady inhalation). In their work, only the total deposition in a replicate of nasal cavity was analysed versus inhalation flow rate, the time-dependent deposition characteristic along the nasal cavity was not discussed.

This study aims to investigate the time-dependent particle deposition under unsteady inhalation in comparing to that of its equivalent steady inhalation flow rate. The unsteady inhalation profile having a tidal volume of 500ml (Hauermann *et al.* 2001) is used. Only inhalation is studied that the exhalation is beyond the scope of this work. The inspiratory period is halved to 1.4s. Two particle sizes of 5 μ m and 20 μ m are studied to reflect a low and high Stokes numbered particle, respectively.

METHOD

Computational Model Construction

The nasal cavity geometry was obtained through a Computed Tomography (CT) scan of the nose of a healthy 25-year-old male Asian (175cm height and 75kg mass). The CT scan was performed using a CTI Whole Body Scanner (General Electric). The single-matrix scanner was used in helical mode with 1-mm collimation, a 40-cm field of view, 120kV peak and 200mA. The scans captured outlined slices in the X-Y plan at different positions along the Z-axis from the entrance of the nasal cavity to just

anterior of the larynx at interval of 1mm to 5mm depending on the complexity of the anatomy. The coronal-sectioned scans were imported into a three-dimensional (3-D) pre-processing software called GAMBIT which created smooth curves by connecting points on the coronal sections. Due to the irregularity of the geometry, unstructured tetrahedrons were created for the mesh. The nasal cavity comprises of 3 regions – Anterior Region (nasal vestibules), Middle Region (olfactory turbinates) and Posterior Region (nasopharynx) as shown in Figure 1.

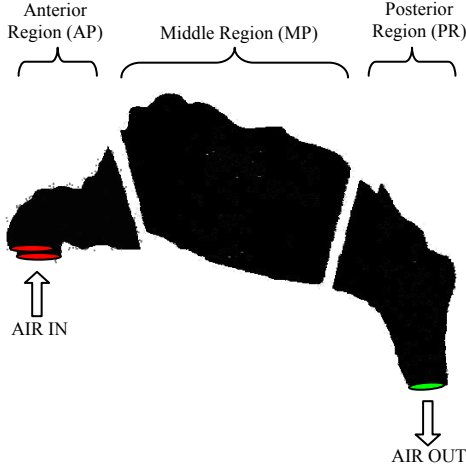


Figure 1: Schematic diagram of Nasal cavity model

An initial model with 260,000 unstructured tetrahedral cells was refined until the skewness of the cells and Y_{plus} value on the walls dropped below 0.8 and 0.78 respectively. The final model consisted of 6.5 million cells which required the use of a HPxw 16Gb RAM, 8 processor workstation to perform the simulations.

Numerical Modelling

Air movement through the nasal cavity is induced by the pressure difference initiated by the thoracic diaphragm at the bottom of ribcage. Thus, an unsteady negative pressure profile relative to the atmospheric pressure at nostril inlet is applied near the larynx to induce the inhalation. The inhalation profile was amended based on the inhalation profile measured from a healthy 50-year-old male volunteer (70kg weight, 170cm height) conducted by Häußermann *et al.* (2001). The inhalation profile has a maximum inhalation flow rate of 20L/min (corresponding to tidal volume of 500mL). However, considering the period of the inspiratory cycle is 2.8s which is about the same as a complete breathing period, the inspiratory period has been halved to 1.4s. The unsteady inhalation flow rate is thus re-adjusted in order to maintain the same tidal volume. The amended inhalation profile is presented in Figure 2 which has a maximum inhalation flow rate of 40.3L/min. For its equivalent steady inhalation flow rate, the inspiratory cycle is time-averaged and is presented by a constant flow rate of 24.6L/min.

The CFD package, ANSYS FLUENT was used to solve the unsteady incompressible fluid flow in the nasal cavity. The unsteady Reynolds-averaged mass continuity and momentum equations for the gas phase (air) are given in Eqn. (1) and (2) respectively.

$$\frac{\partial \rho}{\partial t} + \nabla \cdot (\rho \bar{U}) = 0 \quad (1)$$

$$\frac{\partial \rho \bar{U}}{\partial t} + \nabla \cdot (\rho \bar{U} \bar{U}) = -\nabla p + \nabla \cdot (\mu + \mu_t) \quad (2)$$

$$\left(\nabla \bar{U} + (\nabla \bar{U})^T - \frac{2}{3} \delta_{ij} \nabla \cdot \bar{U} \right) + \rho g + \bar{F}$$

where $\mu_t = \rho \alpha^* \frac{k}{\omega}$; $\delta_{ij} = 1$ if $i = j$ and $\delta_{ij} = 0$ if $i \neq j$;

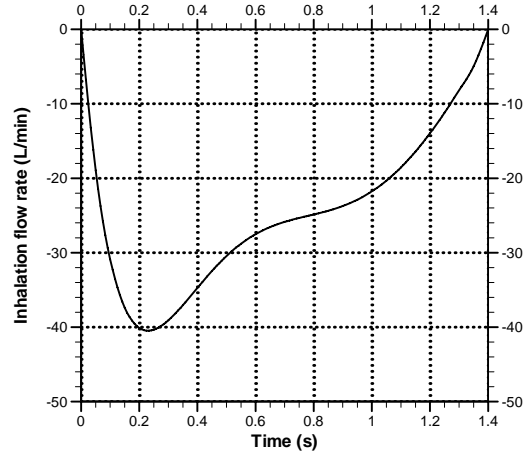


Figure 2: Pressure profile for the Inspiratory cycle

The QUICK scheme was employed to solve the momentum equation; while SIMPLEC method was used to resolve pressure-velocity coupling. Although the Reynolds number at the nostril inlets at the peak inhalation rate of 40.3L/min is 2,250, the high degree of irregularity contributes to instabilities enhancing the transition to turbulent. Thus, the low-Reynolds Shear Stress Transport (SST) $k-\omega$ turbulent model was used to close the Reynolds averaged equations in Eqn. (1) and (2). The equations for turbulent kinetic energy, k , and the specific dissipation rate, ω , are given in Eqn. (3) and (4) respectively.

$$\frac{\partial}{\partial t} (\rho k) + \nabla \cdot (\rho \bar{U} k) = \nabla \cdot \left[\left(\mu + \frac{\mu_t}{\sigma_k} \right) \nabla k \right] + \tilde{G}_k - Y_k + S_k \quad (3)$$

$$\frac{\partial}{\partial t} (\rho \omega) + \nabla \cdot (\rho \bar{U} \omega) = \nabla \cdot \left[\left(\mu + \frac{\mu_t}{\sigma_\omega} \right) \nabla \omega \right] + \tilde{G}_\omega - Y_\omega + D_\omega + S_\omega \quad (4)$$

The particle trajectory was modelled by using a Lagrangian approach and integrating the force balance equations on each particle as follows.

$$\frac{du_p}{dt} = F_D (u_g - u_p) + \frac{g(\rho_p - \rho_g)}{\rho_p} + F_S \quad (5)$$

where

$$F_D = \frac{18 \mu_g C_D \text{Re}_p}{\rho_p d_p^2 24} \quad (6)$$

$$\text{Re}_p = \frac{\rho_p d_p |u_p - u_g|}{\mu_g} \quad (7)$$

$$C_D = a_1 + \frac{a_2}{\text{Re}_p} + \frac{a_3}{\text{Re}_p^2} \quad (8)$$

in which a 's are the empirical constants for smooth spherical droplets over several ranges of droplet Reynolds number Morsi and Alexander (1972). The second term in Eqn.(5) is the gravity term while the third term, F_S represents other possible forces such as virtual mass force, Basset force, pressure gradient force, lift force, thermophoretic force and Brownian force. The CFD code handles the turbulent dispersion of droplets by integrating

the trajectory equations for individual droplets, using the instantaneous fluid velocity, $u_i^g + u_i(t)$, along the droplet path during the integration process. Here, the Discrete Random Walk model (DRW) is used where the fluctuating velocity components u_i that prevail during the lifetime of the turbulent eddy are sampled by assuming that they obey a Gaussian probability distribution. A near wall correction was applied to account for the anisotropic behaviour of turbulence by damping the turbulent kinetic energy as described in Matida *et al.* (2004).

A total number of 10,000 particles were released passively at surfaces parallel to the nostrils and which was 5% smaller in diameter than nostrils to avoid immediate particle deposition. Zero injection velocity was set to allow particles to move and deposit based on the induced pressure difference at each time step. All particles were assumed to be injected passively at 0s. Moreover, it is assumed that the particle will not affect the fluid flow (one-way coupling) as the volume fraction of the droplets was relatively low (<10%). Other assumptions include:

- i) no particle rebounding off the walls/surfaces;
- ii) no particle coagulation in the particle deposition process; and
- iii) all particles are spherical and non-deforming.

It is known that the sphericity of particle affects the drag coefficient and results in different deposition efficiency. Changes in drag coefficient due to different shapes of particles may refer to Loth (2008) and Tran-Cong (2004) for details.

RESULTS AND DISCUSSION

Validation

Since experimental studies regarding the unsteady inhalation are limited in the literature, both pressure difference between nostrils and nasopharynx and the deposition efficiency for the present nasal cavity model were validated with steady inhalation.

The averaged pressure differences at different inhalation flow rates reported by Kelly *et al.* (2004) and Weinhold and Mlynski (2004) was compared with present model which were measured based on a constant inhalation rate. The steady inhalation at 24.6L/min and the peak inhalation rate of 40.3L/min from the unsteady inhalation gave an averaged pressure difference of 34.8Pa and 83Pa respectively. It was found that the present model is in excellent agreement with other studies (see Figure 3).

Monodispersed particles in the range of 1-50 μ m were released passively into the nasal cavity model under flow rates of 5, 10, 15 and 20L/min. The deposition of particles as a function of the inertial parameter, ($d_a^2 Q$) is shown in Figure 4 which displays the characteristic curve associated with inertial deposition. Differences in deposition may be attributed to the inter-subject variability between the nasal cavity models obtained by Kelly *et al.* (2004) (53 year-old Caucasian male) with the model used in the present study (25 year-old Asian male) while Häußerman *et al.* (2001) also states that nasal cavity replicate casts with wider airways can cause less deposition due to secondary flow. A curve fit is applied to the simulated data which produces:

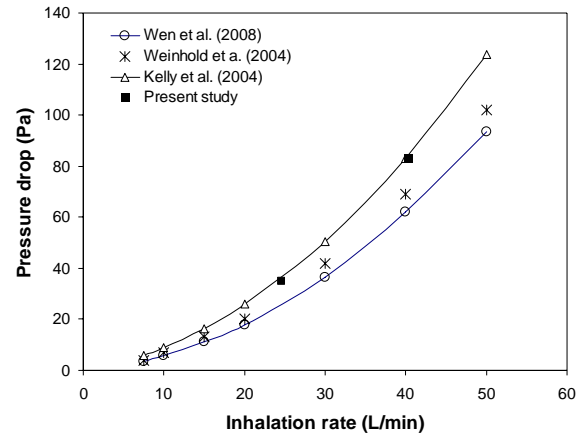


Figure 3: Pressure drop across the human nasal cavity as a function of inhalation flow rate compared with reported experimental works (Kelly *et al.* 2004; Weinhold and Mlynski 2004) and a numerical study (Wen *et al.* 2008)

$$\eta = 1 - \exp\left(-(\alpha \cdot d_a^2 Q)^\beta\right) \quad (9)$$

where the coefficients are, $\alpha = 2.7e-5$, $\beta = 1.05$.

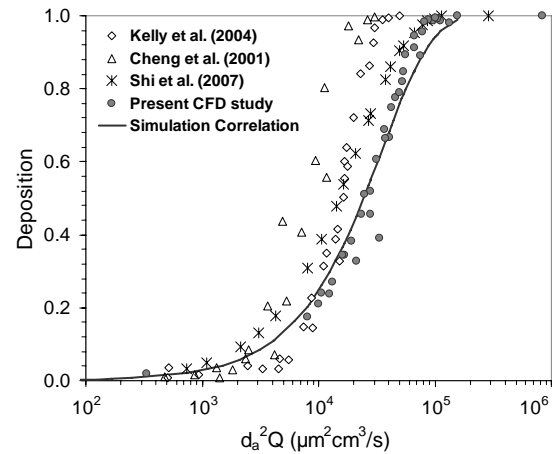


Figure 4: Total deposition of particles against inertial parameter compared with reported data

Particle Deposition

The unsteady deposition efficiency is presented at an interval of 0.1s. For those deposited particles during 0s to 0.1s will contribute to the deposition efficiency at 0.1s. Based on this presentation method, the deposition efficiencies versus time for 5 μ m and 20 μ m are shown in Figure 5 and Figure 6 respectively. The highest deposition of these two particle sizes is found in the middle region and then followed with the anterior region. As the inhalation develops, particles start to deposit in the posterior region. During the inspiratory cycle, deposition of 5 μ m particles occurs in the first 0.9s; while no 20 μ m particle is deposited after 0.2s. Such zero deposition of 20 μ m is due to high deposition efficiency at low inhalation rate at or before 0.1s and in absence of further inhalation of particles.

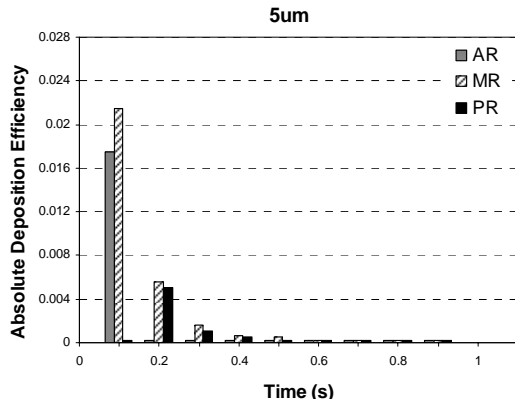


Figure 5: Absolute deposition of 5µm particle

From the view of escape efficiency, 5µm particle has about 3 times higher than that of 20µm (see Figure 7). The possible reason for this significant different in escape efficiency is due to different particle transport phenomenon. For large particles, particle inertia tends to dominate particle movement and reduces its dependence to the airflow (i.e. inertial deposition); vice versa, smaller particles are more dependent on the structure of airflow (i.e. sedimentation deposition). Since the relaxation time of particle increases with particle sizes, local eddies do not impose as strong influence on larger particles as it does on small particle. As the result, stronger inhalation flow rate leads to higher escape efficiency for small particles.

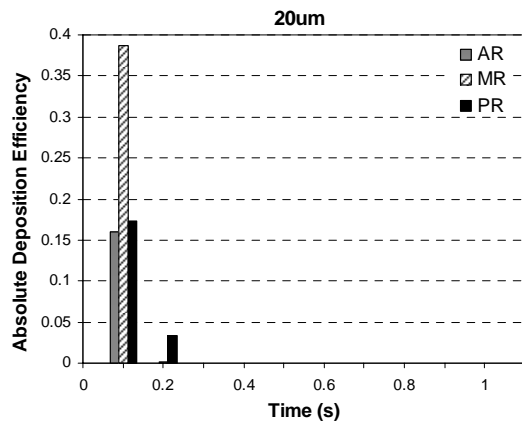


Figure 6: Absolute deposition of 20µm particle

The time-dependent particle deposition behaviour in conjunction with time is investigated through the relative deposition which is defined by Eqn. (10) in which $N_{deposited}$ is the total number of particle deposited in the nasal cavity at a time step; while $N_{suspended}$ is the number of particles suspending in air at the same time step.

$$DE = \frac{N_{deposited}}{N_{suspended}} \quad (10)$$

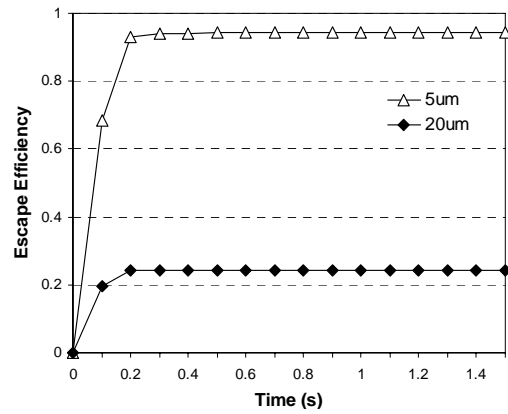


Figure 7: Escape efficiencies of 5µm and 20µm

Based on this equation, the relative deposition efficiency for 5µm and 20µm are given in Figure 8. Based on the inhalation profile adopted in present study, it is found that the inhalation rate promotes higher deposition efficiency for 5µm particle than 20µm particle. Doubling the inhalation rate of 0.1s at 0.2s leads to a rise of about 36% in escape efficiency for 5µm particles and about 25% for 20µm particles. It implies that higher inhalation flow rate prohibits deposition of small particles than large particles. This finding is in line with the one of general findings with steady inhalation that high inhalation discourages deposition of small particles than large particles. Besides, Schroeter *et al.* (2006) also obtained the similar trend that higher inhalation flow rate promotes lower deposition for smaller particles. As shown in Figure 8, the increment in the inhalation rate at 0.2s does not enhance the deposition efficiency of 20µm particle; but a significant rise in 5µm particle is found.

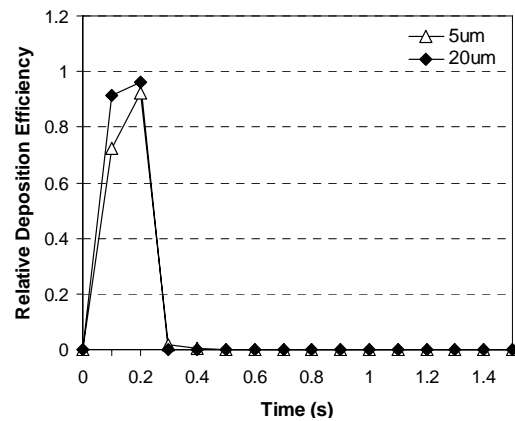


Figure 8: Relative deposition efficiency

The cumulative deposition efficiency is defined as the ratio of the total number of particles deposited in each region of nasal cavity to the total number of particles released. The cumulative efficiencies per region for 5µm and 20µm particles are presented in Figure 9 and Figure 10 respectively. General speaking, the middle region received the highest deposition for both 5µm and 20µm particles. The figures also clearly show that higher deposition efficiency was found in posterior region than anterior region for 20µm particle; while 5µm particle is in other way round. Interestingly, deposition of 5µm in the PR has a time lag of at least 0.1s.

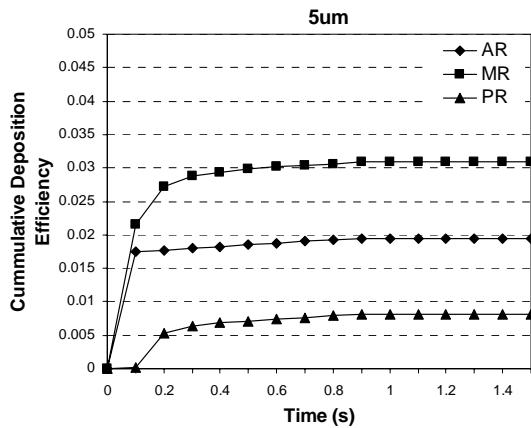


Figure 9: Cumulative deposition of 5µm

The deposition of 5µm particle in the PR starts at 0.2s; while immediate deposition occurs for the 20µm particle in particular at the rear part of the nasopharynx. Since the deposition mechanism for these two particle size are different, they come to different results. As aforementioned, small size particles dominate by sedimentation deposition and large size particles by inertial deposition. In the presence of the bend near nasopharynx in the airway, flow separation occurs and eventually, the 20µm particles deposit by inertial deposition. In the absence of further inhalation of particles, the first 0.2s is more crucial in deposition efficiency for 20µm under the amended inhalation profile.

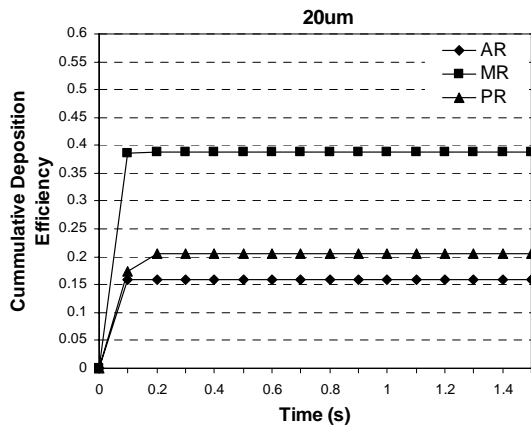


Figure 10: Cumulative deposition of 20µm

Deposition under Steady versus Unsteady inhalations

The total deposition efficiencies between steady and unsteady inhalations are compared in this section. A steady flow rate of 24.6L/min is used, which is equivalent to the time-averaged unsteady inspiratory cycle shown in Figure 2. The comparison between the deposition efficiencies obtained under steady and unsteady inhalations of 5µm and 20µm are presented in Figure 11 and Figure 12 respectively. Surprisingly, the deposition efficiencies of 5µm particle at steady and unsteady inhalations are very similar which give the total deposition of 8% for steady inhalation and 5.5% for unsteady inhalation. Among the regions, unsteady inhalation results in about 17%~50% less in the deposition of 5µm; while for the 20µm particle, the total deposition efficiency is 97% and 75% under steady and unsteady inhalation respectively. The distribution of deposited 5µm particles along the nasal cavity is similar in

these inhalation profiles that highest deposition is still found in middle region. However, the deposition efficiencies of 20µm particles under steady inhalation come to different distribution among regions due to unsteady inhalation. Highest deposition is found in anterior region for steady inhalation; while middle region for unsteady inhalation. Moreover, the deposition efficiency in PR under steady inhalation is found to be triple of that with unsteady inhalation; similar finding is found in AR in other way round.

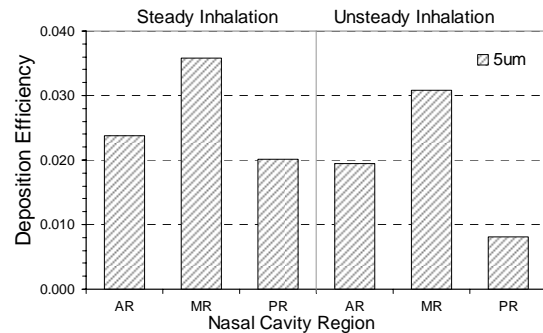


Figure 11: Deposition efficiency for 5µm

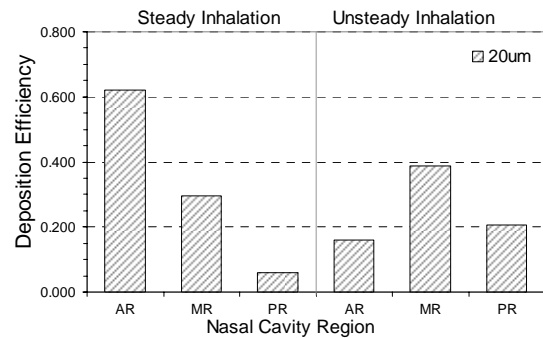


Figure 12: Deposition efficiency for 20µm

Such overestimation in particle deposition under steady inhalation was also found in the works conducted by Häußerman *et al.* (2001), but the overestimation diminished when particle size became larger. However, in present study, the magnitude exaggerates with increasing particle size. In Häußermann *et al.* (2001), the particle sizes studied (1~10µm) that may be too limited to arrive a generic conclusion. In addition, the topologies of the nasal cavity models are different and different locations of local eddies lead to different deposition efficiency.

For the large particle (e.g. 20µm), the deposition in the first 0.2s is nearly 89% of the total deposition (see Figure 9). Thus, the initial airflow structure determines the deposition of large particle. Changes in airflow do not influence the movement of large particle as significant as that acting on small particle. Therefore, with initially higher airflow velocity, steady inhalation promotes particle deposition in AR. In contrast, the inhalation rate was initially lower in unsteady inhalation. Therefore, more particles deposit in the middle region. In overall, the deposition is higher under steady inhalation than unsteady inhalation.

However, Gurman *et al.* (1984a, 1984b) had concluded in other way round. The deposition efficiencies under both steady and unsteady inhalations in tracheobronchial tree were studied. They found that the unsteady inhalation

enhances deposition compared to steady inhalation. A more quantitative had been reported by Landahl (1950) that the deposition under unsteady inhalation was found to be increased by about 15% for inertial deposition and decreased by 22% for sedimentation deposition. Further investigation for other particle sizes will be done in future with wider range of particle size.

CONCLUSION

Time-dependent deposition efficiencies of 5 μm and 20 μm particles in a realistic nasal cavity were investigated by CFD techniques. An unsteady inhalation profile of a realistic breathing cycle measured by Häußermann *et al.* (2001) with halve inhalation period was adopted. The modified unsteady inspiratory cycle has a peak inhalation rate of 40.3L/min. Particles were released passively at 0s. Three profiles of deposition efficiency were presented to discuss the temporal deposition phenomenon. It was found that both particle sizes mainly deposited in the middle region of nasal cavity. Much higher deposition was found in 20 μm particle than that of 5 μm particle. Based on the amended inhalation profile, single passive injection of two particle sizes came to different crucial deposition time. All particles deposited in the first 0.9s of inspiratory cycle for 5 μm particle; while 0.2s for 20 μm particle. As the inhalation develops, escape efficiency was enhanced. The enhancement effect was more significant on low Stokes numbered particles than high Stokes numbered particles. In compared to the steady inhalation, unsteady inhalation led to relatively lower deposition efficiency. The overestimation exaggerated with particle size. In addition, the distribution among regions changed for large particle. However, different conclusions were drawn among limited number of studies, further investigation on the effect of steadiness of inhalation on deposition efficiency in the future is needed.

REFERENCES

ANTHONY T.R., FLYNN, M.R., (2006), Computational fluid dynamics investigation of particle inhalability, *J. Aerosol Sci.*, **37**, 750-765.

BALÁSHÁZY I., HOFMANN, W., (1993), Particle deposition in airway bifurcations — I. Inspiratory flow., *J. Aerosol Sci.*, **24**, 745-772.

CHENG K.H., CHENG, Y.S., YEH, H.C., GUILMETTE, A., SIMPSON, S.Q., YANG, Y.H., SWIFT, D.L., (1996), In-vivo measurements of nasal airway dimensions and ultrafine aerosol deposition in the human nasal and oral airways., *J. Aerosol Sci.*, **27**, 785-801.

GURMAN J.L., LIOY, P.J., LIPPMANN, M., SCHLESINGER, R.B., (1984a), Particle deposition in replicate casts of the human upper tracheobronchial tree under constant and cycle inspiratory flow I: Experimental, *Aerosol Sci. Technol.*, **3**, 245-252.

GURMAN J.L., LIOY, P.J., LIPPMANN, M., SCHLESINGER, R.B., (1984b), Particle deposition in replicate casts of the human upper tracheobronchial tree under constant and cycle inspiratory flow II: Empirical model, *Aerosol Sci. Technol.*, **3**, 253-257.

HÄUßERMANN S., BAILEY, A.G., BAILEY, M.R., ETHERINGTON, G., YOUNGMAN, M.J., (2001), The influence of breathing patterns on particle deposition in a nasal replicate cast., *J. Aerosol Sci.*, **33**, 923-933.

INTHAVONG K., TIAN, Z.F., LI, H.F., TU, J.Y., YANG, W., XUE, C.L., LI, C.G., (2006), A numerical

study of spray particle deposition in a human nasal cavity, *Aerosol Sci. Technol.*, **40**.

KELLY J.T., ASGHARIAN, B., KIMBELL, J.S., B.A., W., (2004), Particle deposition in human nasal airway replicas manufactured by different methods. Part 1: Inertial regime particles., *Aerosol Sci. Technol.*, **38**, 1063-1071.

LANDAHL H., (1950), On the removal of airborne droplets by the human respiratory tract: I. The lung, *Bull Math Biophys*, **12**, 43-56.

LOTH E., (2008), Drag of non-spherical solid particles of regular and irregular shape. *Powder Technology* **182**, 342-353.

MATIDA E.A., FINLAY, W.H., LANGE, C.F., GRGIC, B., (2004), Improved numerical simulation fo aerosol deposition in an idealized mouth-throat, *J. Aerosol Sci.*, **35**, 1-19.

MORSI S.A., ALEXANDER, A.J., (1972), An investigation of particle trajectories in two-phase flow systems., *J. Fluid Mech.*, **55**, 193-208.

MOSKAL A., GRADON, L., (2002), Temporary and spatical deposition of aerosol particles in the upper human airway during breathing cyclr, *J. Aerosol Sci.*, **33**, 1525-1539.

SCHROETER J.D., KIMBELL, J.S., ASGHARIAN, B., (2006), Analysis of particle deposition in the turbinate and olfactory regions using a human nasal computational fluid dynamics model, *J. Aerosol Med.*, **19**, 301-313.

SE C.M.K., INTHAVONG, K., TU, J.Y., (2009), Inhalability of Micron Particles through the Nose and Mouth, *Inhal. Toxic.*, Submitted.

SHANLEY K.T., ZAMANKHAN, P., AHMANDO, G., JHOPKE, P.K., CHEUNG, Y.S., (2008), Numerical simulations investigating the regional and overall deposition efficiency of the human nasal cavity, *Inhal. Toxic.*, **20**, 1093-1100.

SHI H.W., KLEINSTREUER, C., ZHANG, Z., (2007), Modeling of inertial particle transport and deposition in human nasal cavities with wall roughness, *J. Aerosol Sci.*, **38**, 398-419.

SUBRAMANIAM R.P., RICHARDSON, R.B., MORGAN, K.T., KIMBELL, J.S., GUILMETTE, R.A., (1998), Computational fluid dynamics simulations of inspiratory airflow in the human nose and nasopharynx., *Inhal. Toxic.*, **10**, 91-120.

TRAN-CONG S., Gay, M., Michaelides, E.E., (2004), Drag coefficients of irregularly shaped particles. *Powder Tech* **139**, 21-32.

WEINHOLD I., MLYNSKI, G., (2004), Numerical simulation of airflow in the human nose, *Eur. Arch. Otorhinolaryngol.*, **261**, 452-455.

WEN J., INTHAVONG, K., TU, J.Y., WANG, S., (2008), Numerical simulations for detailed airflow dynamics in a human nasal cavity, *Respir. Physiol. Neurobiol.*, **161**, 125-135.

ZHANG Z., KLEINSTREUER, C., KIM, C.S., (2009), Comparison of analytical and CFD models with regard to micron particle deposition in a human16-generation tracheobronchial airway model, *J. Aerosol Sci.*, **40**, 16-28.

ZWARTZ G.J., GUILMETTE, R.A., (2001), Effect of flow rate on particle deposition in a replica of a human nasal airway., *Inhal. Toxic.*, **13**, 109-127.